Numerical simulation of the flow past a rotating propeller behind a hull

Roberto Muscari, Andrea Di Mascio

Italian Ship Model Basin (CNR-INSEAN), Rome, Italy

ABSTRACT

Aim of this work is the analysis of the flow in the stern region of a fully appended twin–screw hull by an URANSE simulation. The numerical tool consists of a finite volume code, where the convective terms are integrated by a third–order algorithm that, introducing a very small numerical diffusivity, permits to follow the evolution of the tip vortices and their interaction with the rudder. The movement of the propeller is resolved by a dynamic overlapping grids method. The numerical data are first verified and validated by comparison with measurements and then exploited in order to get a deep insight of both the velocity field and the pressure oscillation on the stern vault.

Keywords

Unsteady RANSE, dynamic overlapping meshes, propeller-hull interaction.

1 INTRODUCTION

This work represents a sequel of the paper presented at the first Symposium on Marine Propellers (SMP'09) (Muscari & Di Mascio 2009). On that occasion, the simulation of the turbulent, viscous flow around a non-cavitating isolated propeller was performed by an Unsteady Reynolds Averaged Navier–Stokes Equations (URANSE) code featuring dynamic overlapping grid capabilities, and some preliminary results on a very coarse mesh were also shown for the present test case geometry. We are now able to provide the numerical results for a finer, more regular mesh that allows us to study in detail the flow field characteristics.

The analysis of the flow around a rotating propeller behind a hull has great relevance with respect to several point of views. In particular, the following ones can be highlighted:

- the main source of noise on a ship is the propulsion system and the accurate prediction of the flow features in the stern region in terms of inflow to the propeller, evolution of the vortical structures and their interaction with the appendages (in particular the rudder), pressure oscillations on the stern vault, represent an important step in the effort for improving the on–board comfort and reduce the radiated noise.

- the interaction of the wake of the propellers with the rudders is also important in respect to the performance of the control surfaces; the fore–knowledge of the velocity and pressure fields around the rudders placed downstream the rotating propellers can help to design a ship with better manoeuvrability characteristics, whereas overlooking such information can lead to very poor results.

- numerical results of the viscous flows past the propeller are necessary in order to understand the interaction with the hull form to determine both global forces, such as resistance and propulsive power, and local flow characteristics, such as wave profiles in the stern region.

- the data collected by these numerical studies, both in straight course and with relevant values of yaw or roll angles, would form a valuable data set for the construction and validation of an interactive approach, where the role of the propeller is mimicked by a body-force distribution without solving for the details of the turbulent flow around the rotating propeller blades.

In this work, we present the analysis of the turbulent flow past a fully appended, twin screw hull moving in straight course, carried out by numerical integration of URANSE. To this purpose, the RANSE code developed at INSEAN was used for the simulations. The latter were performed on two grids level, a fine one composed by 12.7M cells and a medium one obtained by taking every other point from the finer mesh (approximatively 1.6M cells). Results are shown in terms of velocity fields in the longitudinal plane containing the symmetry plane of the rudder and the axis of the propeller shaft, and in two transversal planes, namely downstream the propeller and downstream the rudder. In these planes, measurements are also available and used in order to validate the computations. Furthermore, the pressure fields on the blades of the propeller are considered in order to understand the different load conditions each single blade goes through during one revolution. Finally, the Fourier analysis of the pressure signal on the stern vault that provide useful information on the harmonic components of radiated noise is performed.

The next section gives an overview of the numerical method, followed by the test case description and the details of the numerical set–up. Then, the results are shown and some final remarks wrap up the paper.

2 NUMERICAL METHOD OVERVIEW

The numerical method is based on the integration of the URANSE, the turbulent viscosity being calculated

by means of a proper turbulence model. The INSEAN code χnavis mplements several turbulence models, ranging from algebraic ones (Baldwin & Lomax 1978, Smagorinsky 1963) to two–equations differential models (Lam & Bremhorst 1981, Chang et al 1995). For the present results, the one–equation model by Spalart & Allmaras (1994) was used.

Proper boundary conditions are enforced at the physical boundaries of the numerical domain. In particular, on the solid walls the velocity of the fluid is set equal to the local velocity of the body; at the inflow, the velocity is set to the undisturbed flow value, whereas at the outflow the pressure is set equal to zero; finally, on the free surface, whose location is determined by a kinematic condition, the continuity of stresses across the surface is enforced (dynamic condition).

The numerical algorithm is based on a finite volume technique with pressure and velocity co–located at cell center. Viscous terms are integrated by a standard second order centered scheme, whereas for the convective and pressure terms three different schemes can be chosen: a second order ENO (Essentially Non Oscillatory) scheme, a third order upwind scheme and a fourth order centered scheme (Di Mascio et al 2008). The third order upwind scheme was used for the computations shown in the following, as it represents the best trade–off between small numerical dissipation and good robustness. Of course, because of the treatment of the viscous terms, the scheme remains formally second order in space.

The simulation of the free–surface is performed by a single–phase level set algorithm (Di Mascio et al 2007). An ENO technique (similar to the one used for the bulk flow) is used to solve the level set equations.

The physical time–derivative in the governing equations is approximated by a second order accurate, three–point backward finite difference formula (Di Mascio et al 2004).

Finally, the rotation of the propeller with respect to the fixed hull is simulated by a dynamic overlapping grids algorithm (Muscari & Di Mascio 2005, Muscari et al 2006).

3 TEST CASE SET-UP

We consider the geometry represented in Figure 1: it is a model of a patrol–like vessel (INSEAN Model C2388A), characterized by a bulbous bow, a transom stern and two inward–turning propellers. The length of the model is $L_{pp} = 5.333$ m and it moves in straight course at a speed $U_\infty = 2.52$ m/s. Consequently, we have a Reynolds number $Rn = 1.18 \times 10^7$ and a Froude number $Fn = 0.348$. The propellers, shown in Figure 2, are two four-bladed, adjustable-pitch, skewed models (INSEAN Model E1630). Their diameter is $D = 0.21$ m and their turning rate is set to $n = 820$ rpm. Hence, the nominal advance coefficient is $J = 0.878$. The geometrical quotes and the operational parameters for both the hull and the propellers are summarized in Tables 1-2.

The computations were performed on two grid levels, the coarser one being obtained by taking every other point of
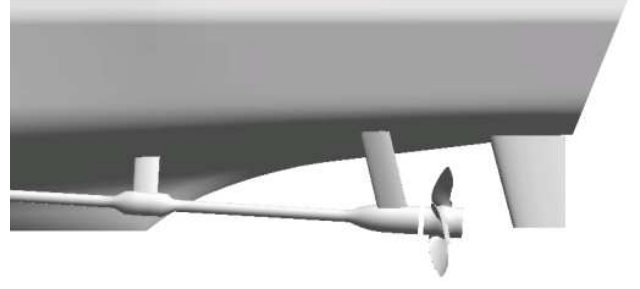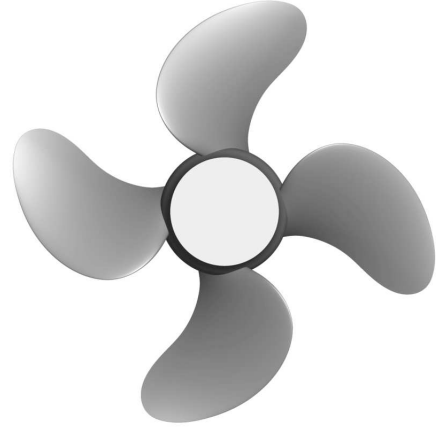

Figure 1: Side view of the hull model

Figure 2: Front view of the propeller model

Table 1: Test hull parameters

INSEAN C2388A model	
Scale ratio	15.0
L_{pp}	5.333 m
Breadth	0.813 m
Draft	0.216 m
Displacement	0.413 m^3
Speed	2.52 m/s
Fn	0.3482
Rn	1.18 10^7

the finer one. All the variables were non–dimensionalized with the length of the model ($L_{pp} = 5.333$ m), the undisturbed flow velocity ($U_\infty = 2.52$ m/s) and a reference density ($\rho_w = 1000$ Kg/m^2). The time step for the fine grid was chosen equal to the time needed by the propeller to perform a half degree rotation (that is, in non–dimensional form, $dt = 0.48 \times 10^{-4}$). Consistently, the non–dimensional time step for the medium grid was 0.96×10^{-4} (one degree rotation time).

Because of the symmetry of the geometrical configuration, we could consider only half hull with the left propeller. The blocks that describe the bare hull and the three-dimensional background (on whose boundaries the far–field boundary conditions are enforced) were made by a relatively small

Table 2: Test propeller parameters

INSEAN E1630 model	
Scale ratio	15.0
Number of blades	4
Diameter	0.21 m
Expanded area ratio	0.468
Pitch ratio (0.7 R)	1.183
Hub ratio	0.295
Turning rate	820 rpm
Nominal advance coefficient	0.878

Figure 3: Detail of the mesh on the surface of the hull

number of cells (Table 3). Most of the cell were dedicated to the propeller (hub and blades) whose components were modelled by separate, overlapping "O"–grids. In order to follow the evolution of the tip vortices and their interaction with the rudder, a high percentage of cells was placed in the wake of the propeller and around the rudder itself. Given the relatively coarse mesh around the bare hull, a refinement block was laid on the stern vault that contained both the rotating propeller and the rudder. The distribution of cells for the modeling of all the different parts of the geometry is reported in Table 3.

Table 3: Distribution of computational cells

Moving blocks	$\%N_{\text{tot}}$
four propeller blades	31.7%
propeller hub	9.8%
Fixed blocks	
propeller wake	16.9%
rudder	16.7%
shaft brackets	10.0%
refinement block	6.6%
propeller shaft	2.6%
hull	4.6%
background	1.1%
Percentage overlap	$\sim 8.0\%$

Figure 3 shows a detail of the mesh on the surface of the hull (the mesh is graphically mirrored in order to render a better idea of the complete geometry). In the figure, different colors are used to represent each part of the overlapping grid. Figure 4, through a cut of the numerical domain, shows a detail of the volume mesh.

With regard to the generation of suitable initial conditions, some comments are necessary. The problem has evidently two different time scales: one associated to the onset and evolution of the wake around the hull, the other dependent on the blade frequency. To obtain a fully developed hull wake by marching in time with the afore–mentioned time–steps would have been unfeasible. For this reason, a pre-
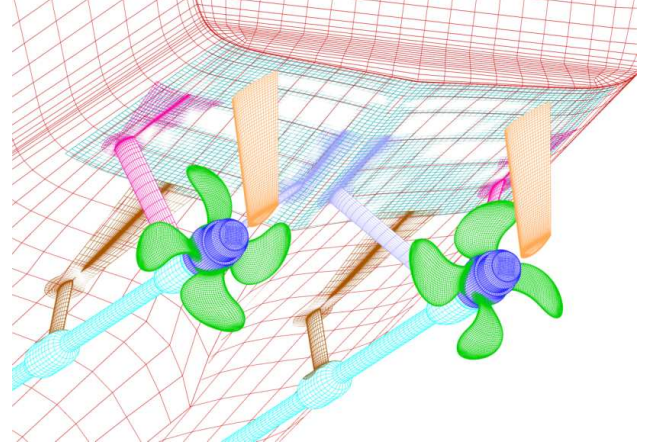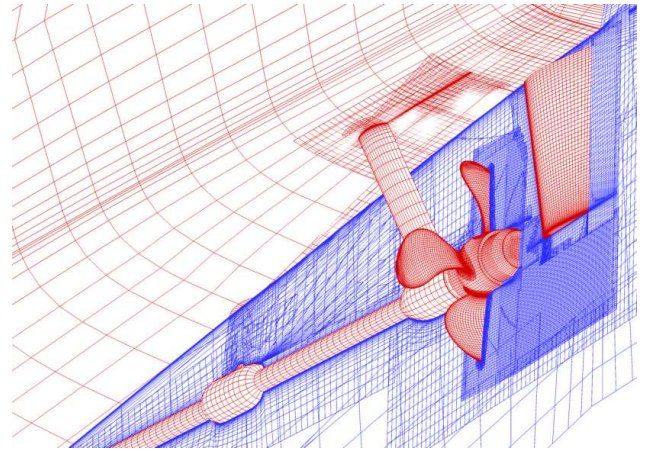

Figure 4: Detail of the volume mesh

liminary steady state computation (i.e. with the propeller kept fixed) was performed in order to obtain a flow field with a fully developed wake of the hull. Starting from this initial condition, the propeller was smoothly accelerated up to its regime speed and, then, the computation proceeded for 13 propeller revolutions.

Grid uncertainty was evaluated according to Roache (1997). In particular, we first estimated the solution variation as

$$E = \frac{f_2 - f_1}{1 - r^p} \qquad (1)$$

where f_1 and f_2 are, respectively, the fine-grid and coarse-grid solutions, r is the refinement factor ($r = 2$, in this work) and p is the *formal* order of accuracy ($p = 2$, for the present code). Then, we evaluated the uncertainty by

$$U_N = F_s \left| E \right| \qquad (2)$$

where F_s is a safety factor that we take, according to Roache, equal to $F_s = 3$.

As to iterative convergence for each sub–step, it was found to be always negligible with respect to grid uncertainty.

4 RESULTS

Before applying the numerical code to the full geometry, in order to gain some confidence in the outcome of the simulation, an isolated propeller in uniform inflow was considered. The test was performed in an inertial frame of reference with the complete geometry of the propeller, in order to reproduce as much as possible the final (i.e. behind the hull) configuration and the results, already reported in (Muscari & Di Mascio 2009), can be summarized by Figure 5:

- the two data sets present a good overall agreement;

- the thrust is well predicted on both meshes for the three values of the advance coefficient;

- the torque, being strongly dependent on viscous forces, is more sensitive to the grid refinement (especially for $J = 1$, hence the higher uncertainty for this point). For the lower values of J, there is a smaller improvement from the coarser to the finer mesh; however, also in the worst case $J = 0.2$, the difference between the experimental value of K_Q and the numerical results on the fine grid is bounded by 4.6%.
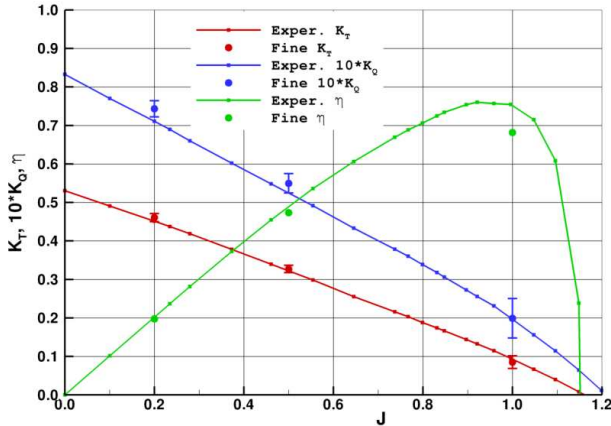

Figure 5: Open water characteristics for INSEAN E1630 model

4.1 Thrust analysis

The full configuration is much more interesting (Figure 6). In this case, the thrust exerted by each blade obviously depends on the azimuthal position, with higher loads during the downward motion and, conversely, smaller thrusts produced during the upward motion. This behavior is caused by the fact that during the downward motion the relative velocity of the incoming flow is higher for two reasons: firstly, because of the tapered stern, the projection of the velocity of the incoming flow on the plane of the propeller is directed towards the top–right angle of the figure; hence, the angle of attack of the blades with respect to the fluid is higher in the bottom–right quadrant. The same effect is produced also by the downward slope (about 3.44°) of the propeller shaft (Figure 1): the longitudinal component of the velocity of the blades during the downward motion is directed towards the bow and the blade experiences a
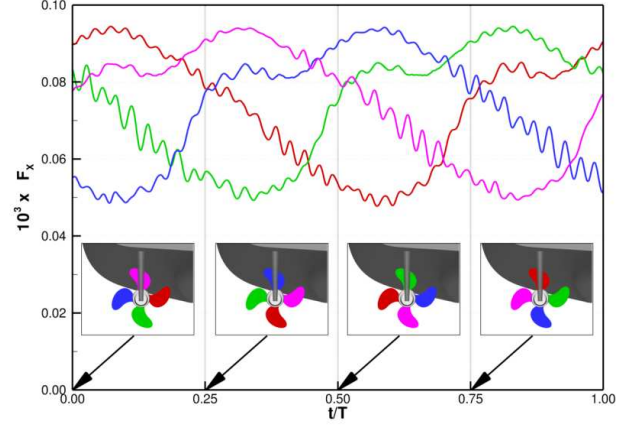

Figure 6: Thrust of the blades during one period

higher relative velocity of the incoming flow. Of course, the opposite holds during the upward motion.

A further analysis of Figure 6 reveals high frequency, high amplitude oscillations in the thrust during the passage from the maximum load to the minimum load conditions. Our opinion is that they depend on the flow separation near the trailing edge of the blade passing through the third quadrant. This separation appears in Figure 7 as an array of relative minima and maxima of the pressure near the trailing edge of the blade in the third quadrant and, to a minor extent, of the blade in the fourth quadrant. Another attempt to visualize the separation phenomenon that gives rise to the thrust oscillations is reported in Figure 8. Here, the vorticity field in the zone around the propeller is shown through the visualization of the iso–contour $\lambda_2 = -22,300$ Hz^2, λ_2 being the second eigenvalue of the tensor $\mathbf{S}^2 + \mathbf{\Omega}^2$ where $\mathbf{S}$ and $\mathbf{\Omega}$ are, respectively, the symmetric and antisymmetric parts of the velocity gradient (Jeong & Hussain 1995). It is evident that the strongest shedding of vorticity takes place in the third quadrant. These trailing vortices diminish in number and align with one another in the fourth and, then, first quadrant, before eventually disappearing in the second sector.

4.2 Velocity field

For the velocity field, experimental data collected at CNR-INSEAN were available (Muscari et al 2010). Measurements were performed in the water channel on a dummy model (INSEAN C2388A) that consisted in the port–side half of the hull, with a rigid plane large enough in order to mimic a symmetry plane for the flow around the complete model. Flow velocity was measured by a two-component back-scatter LDV system and, in particular, the probe was arranged to measure the longitudinal and vertical components of the velocity. Experimental data are available along three cuts of the physical domain: the symmetry plane of the rudder (containing the axis of the propeller shaft), a transversal plane behind the propeller, and a transversal plane behind the rudder.
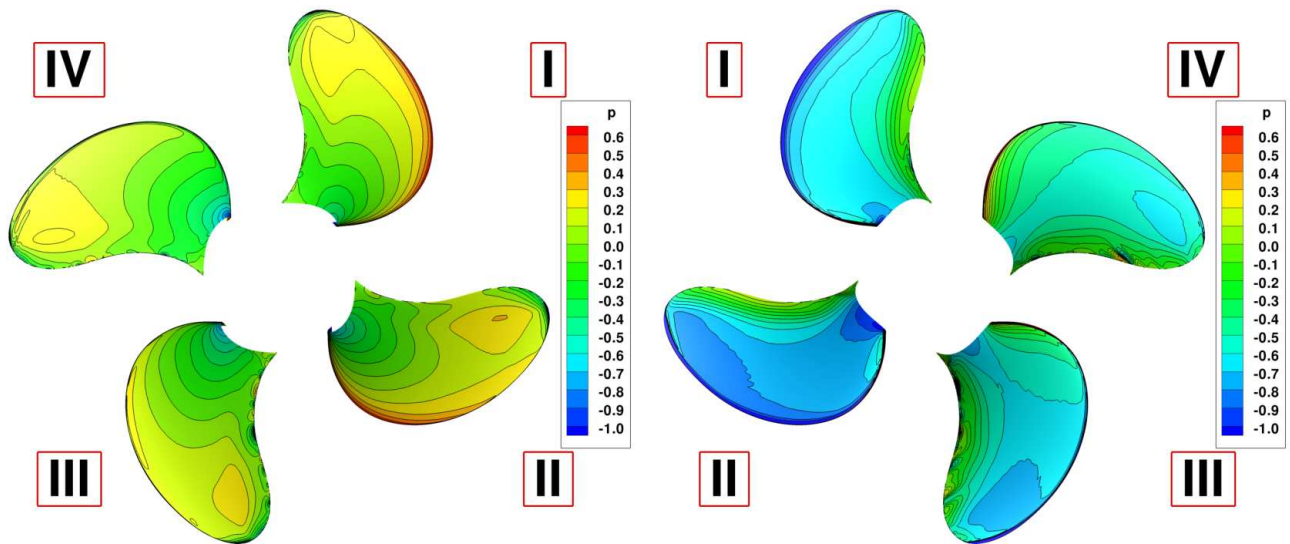
Figure 7: Pressure distribution on the surface of the blades: left, pressure side; right, suction side
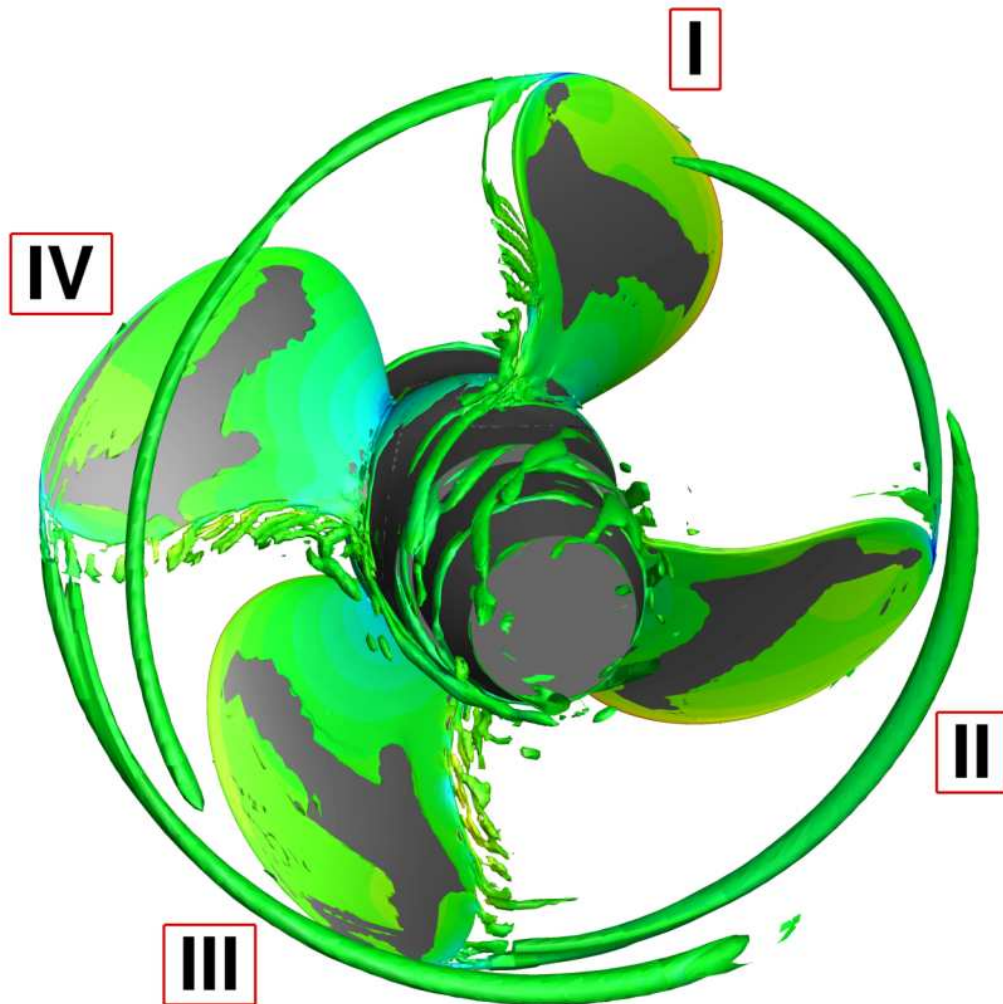

Figure 8: Isoâ$\breve{A}$Ş-surface λ_2 = -22,300 Hz^2 in the near wake of the propeller

Figure 9 shows the longitudinal component of the velocity as predicted by CFD (top) and according to measurements (bottom) in the mid–plane of the rudder. The same comparison in terms of the transversal (i.e. y) component of the vorticity is visualized in Figure 10. The flow fields correspond to the reference position of the propeller (i.e. $\theta = 0°$) but similar agreement is obtained also for other positions. The qualitative agreement between CFD and EFD is quite satisfactory and the main features of the field are captured by the numerical simulation. In particular:
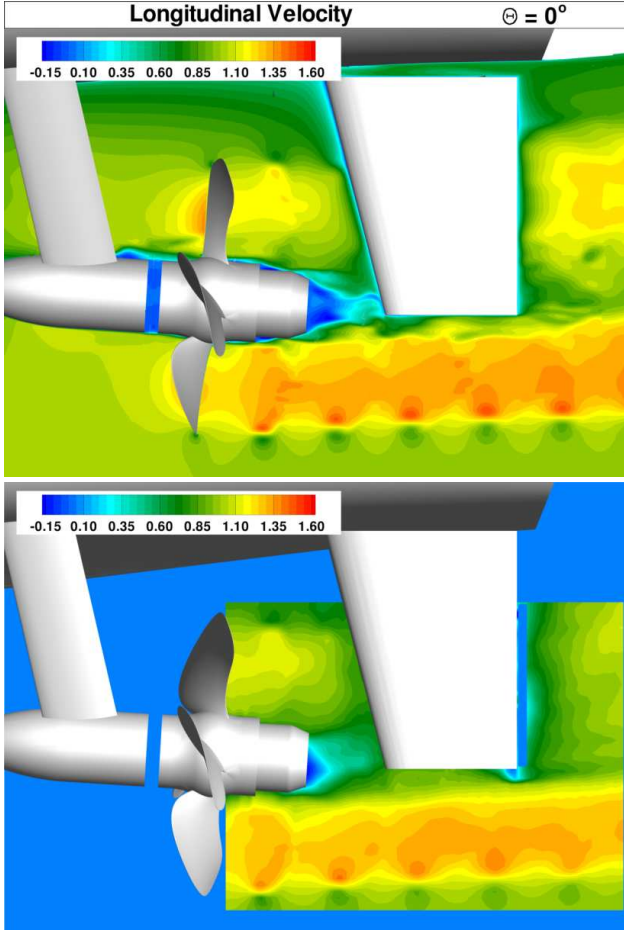
Figure 9: Axial velocity in the mid–plane of the rudder; CFD (top), EFD (bottom)

- the large recirculation zone behind the hub and the sharp, unstable shear layer that separates the inner (slower) flow from the outer (faster) one; this shear layer extends to and eventually impinges on the rudder tip. The recirculation zone is more extended in the CFD field than in the experiments; this is probably caused by a deficiency of the turbulence model that predicts a too low turbulent viscosity and, hence, a low momentum transfer between outer and inner flows.

- the contraction of the propeller stream–tube. This is better seen on the bottom part of the figures where the wake of the propeller is not deformed by the interaction with the rudder. This feature is represented

in both CFD and EFD, that are in excellent mutual agreement.

- the formation and evolution of the tip vortices that, in the upper part of the figures impact on the rudder surface, whereas in the bottom part are freely convected downstream. It is worth noting the ability of the numerical scheme to capture not only the stronger vorticity generated at the tips of the blades but also the vortex shedding from the whole trailing edge, and the strikingly good qualitative agreement between computations and experiments.
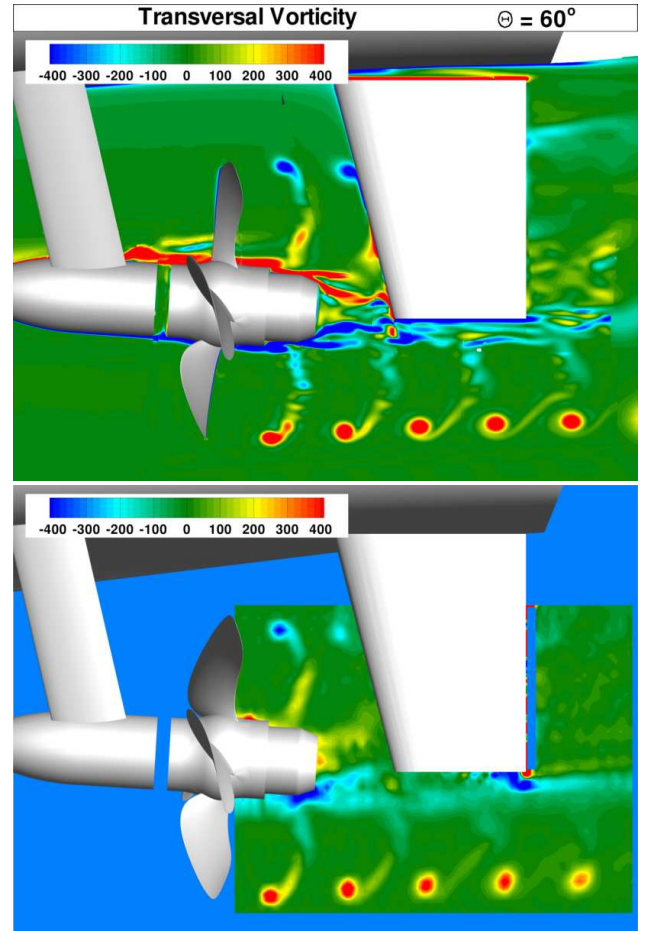

Figure 10: Transversal (i.e. Y-component) vorticity in the mid–plane of the rudder; CFD (top) vs. EFD (bottom)

In order to get a more quantitative comparison between the two data sets, the velocity components are extracted along the white line shown in Figure 11, that is the trajectory followed by the center of the tip vortices in the symmetry plane of the rudder. Figure 12 reports the velocity profiles with the uncertainties for three positions of the propeller, namely $\theta = 0°, 30°, 60°$, (Figure 12). The irregular trend of both experimental and numerical curves is caused by the fact that, the sampling line in Figure 11 being almost parallel to the u-contour lines, a small shift of the sampling line produces appreciable variations of the curves. However, the agreement is quite good and the overlapping between the two curves along the whole region is within the level

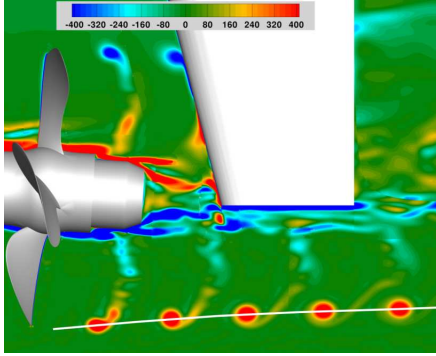of the estimated uncertainties that are (it is worth to note) both rather low (5% at most).

Figure 11: Sample extraction line for results in Figure 12

Numerical and experimental flow fields were also compared also in two transversal cuts downstream of the propeller (cut T3) and behind the rudder (cut T4, see Figure 13).

Results are shown in Figure 14-15 for the reference position of the propeller. The black square in the CFD figures represents the experimental window and was drawn in order to make the comparison easier.

In cut T3, the flow is characterized by a sharp shear layer between the flow accelerated by the propeller and the outer flow. The acceleration is strongest in the lower, innermost quadrant, confirming what already said with regard to the loads on the blades that attain their maximum in this section. It is worth noting the good qualitative agreement between CFD and EFD.

In section T4, the sharp wake of the rudder is the principal feature. A small zone of low velocity, on the suction side near the tip of the rudder, indicates flow separation, probably caused by the interaction of the hub vortices with the appendage. A spanwise misalignment between the flow passing on the suction side and the flow passing on the pressure side is also evident. This indicates different trajectories for the starboard and port tip-vortex filaments, and is a known phenomenon that can be better appreciated in Figure 16. The latter is a representation of the vorticity field past the propeller, obtained through the visualization of the iso–contour $\lambda_2 = -1,116$ Hz^2. For the inward–turning propellers, the tip vortices undergo a progressive deformation while approaching the leading edge of the rudder and, eventually, they are split in two filaments that move on the pressure and suction sides of the appendage before rejoining downstream of it. The interaction with the rudder causes a spanwise displacement of the tip vortex filaments, that is correlated to both the pressure distribution on the rudder and the vortex-wall interaction (Felli et al 2010). The intensity of this misalignment tends to increase chordwise as shown by the isosurface plot of Figure 16. In particular, the spanwise displacement is higher for the filaments moving along the suction side of the rudder, whereas, on the pressure side, the envelope of the tip vortex traces has a
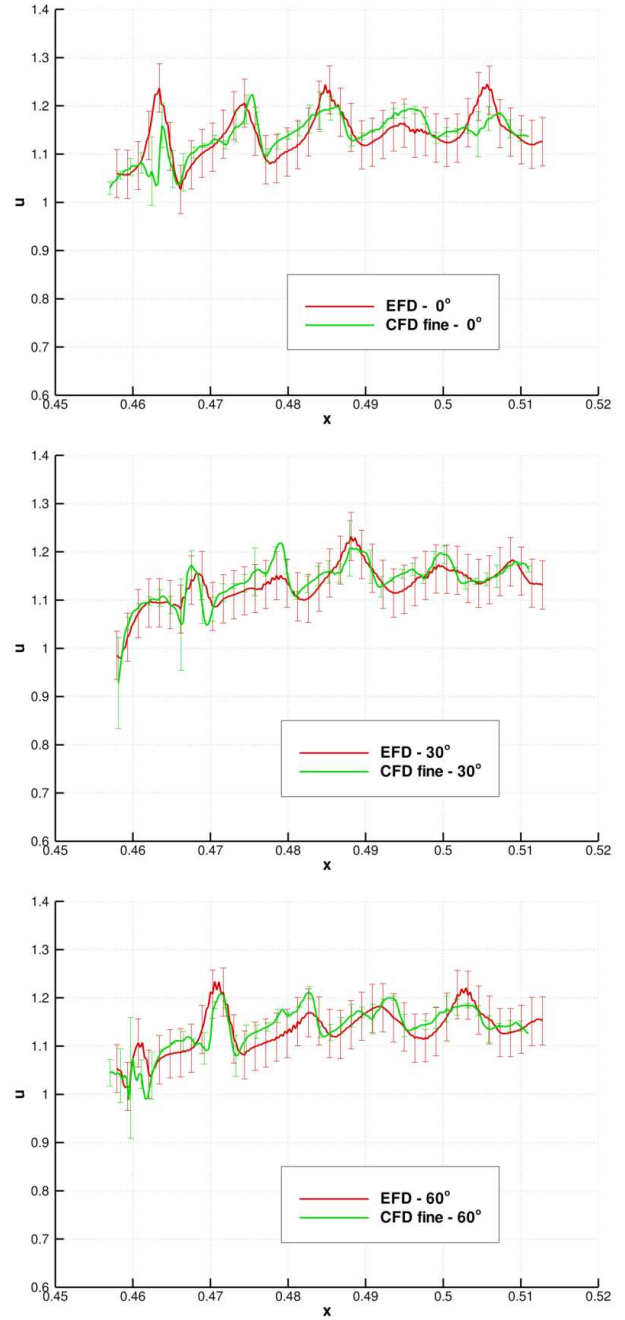

Figure 12: Axial velocity along the line in Figure 11

weaker slope describing a nearly horizontal trajectory. The different behavior of the starboard and port filaments results in the misalignment observed in the transversal plane just behind the trailing edge of the rudder (Figure 15).
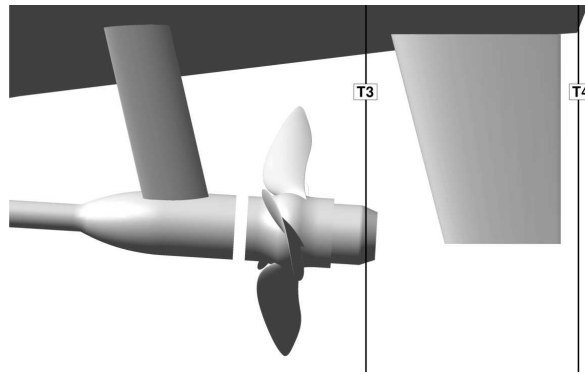
Figure 13: Position of the transversal cuts in the computational field
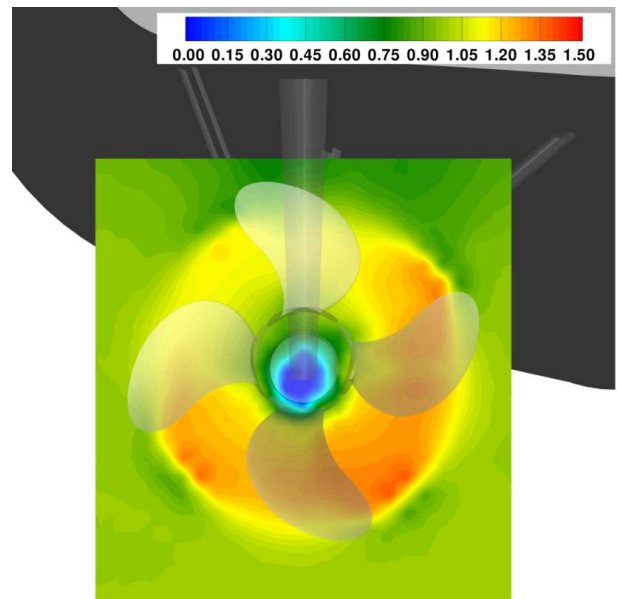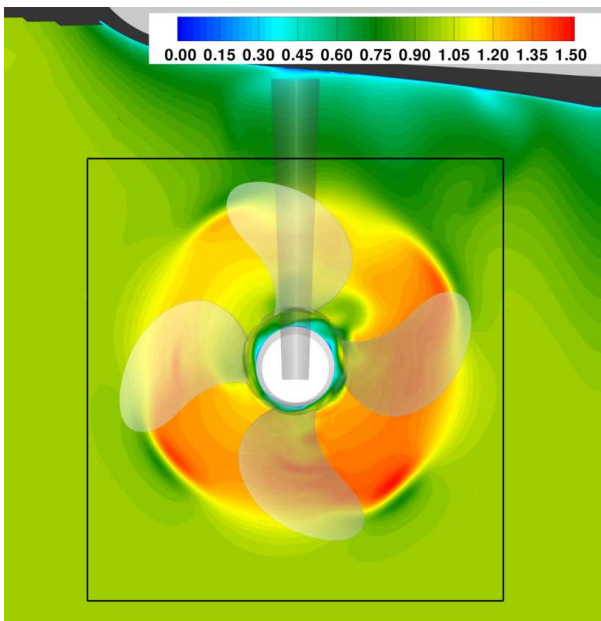

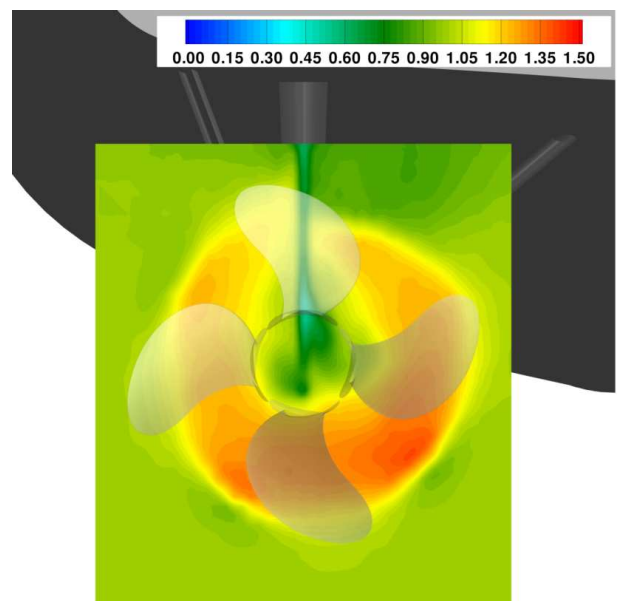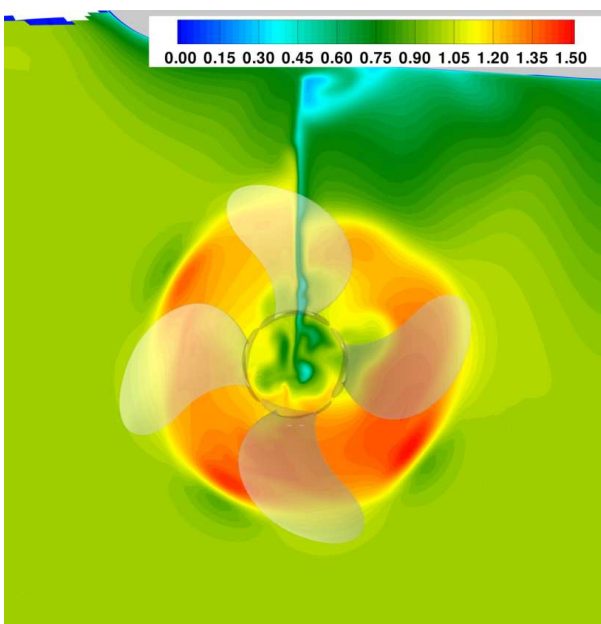Figure 14: Transversal cut T3; Axial velocity, CFD (left) and EFD (right)

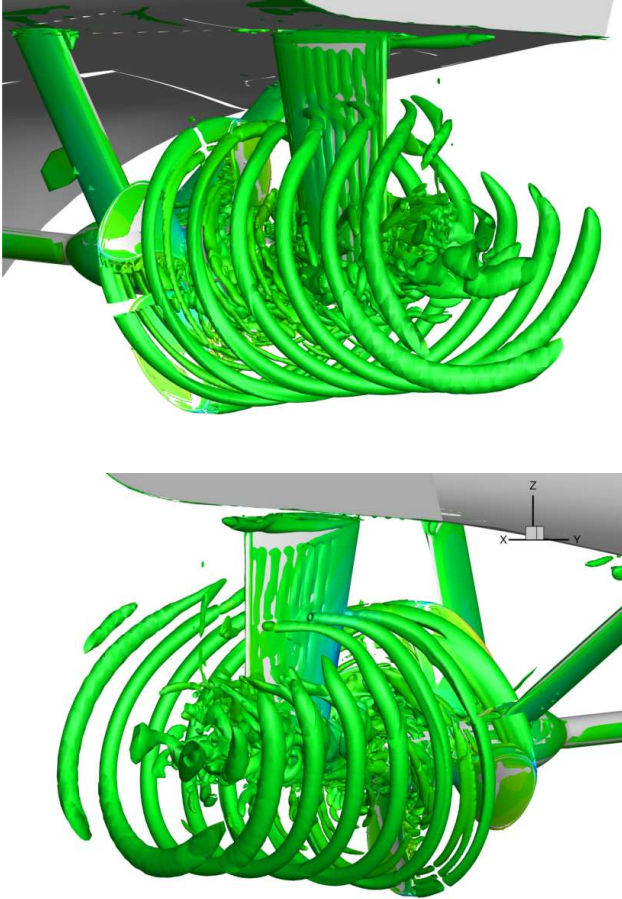Figure 15: Transversal cut T4; Axial velocity, CFD (left) and EFD (right)

Figure 16: IsoâĂŞ-surface $\lambda_2 = $ -1,116 Hz^2; Left: view from the pressure side; right: view from the suction side

clearly not bound to the rotation of the propeller but to a large, highly unstable separation zone near the junction between the bracket and the hull. Apart from these maxima, the fields relative to the first harmonic (corresponding to the shaft frequency) and the second and third ones have no distinctive features. On the contrary, the fourth Fourier coefficient (corresponding to the blade frequency) exhibits a maximum slightly upstream of the propeller plane, indicating that the pressure on the stern vault is strongly influenced by the passage of the blades, and that this influence is more pronounced in the upstream (with respect to the propeller plane) region of the stern. The fifth harmonic has again a flat distribution (with the exception of the zone near the bracket,) and the next harmonic with a significant content is the eighth one (that is, corresponding to twice the blade frequency).
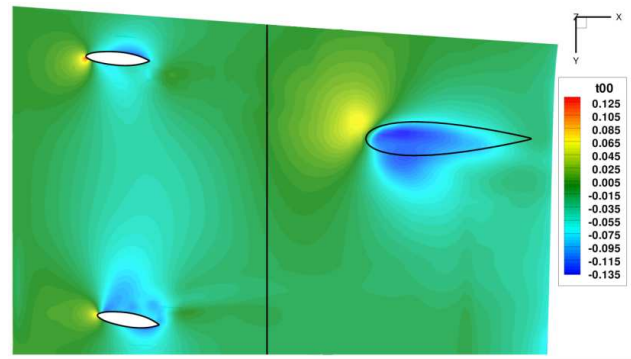

Figure 17: Average value of the pressure on the stern vault

4.3 Pressure fluctuations on the stern vault

For the hydroacoustic analysis of the noise generated by a rotating propeller behind a hull, it is often desirable to know the pressure fluctuations generated by the propeller on the nearby geometries, in particular, on the stern vault which is the source for the greatest part of diffracted noise. As an example of the possibilities offered by CFD in this respect, the average value of the pressure together with the main harmonics of the periodic signal are drawn in Figure 17.

In order to analyze the pressure field, the distribution on the surface of the hull was sampled every step (that is, every half degree of revolution of the propeller) obtaining 720 pressure samples for each cell. Then, the Fourier transform of the (almost periodic) signal was computed at each point and the modulus of the first Fourier coefficients drawn in the figures. The black lines represent the propeller plane, the junctions of the aft-brackets with the hull, and the projection of the top of the rudder on the hull. The symmetry plane of the hull is on the bottom part of the figures. As expected, the average pressure reaches the maximum values near the leading edge of the brackets and of the rudder, whereas a moderately low pressure zone extends between the brackets. The analysis of the higher harmonics reveals a zone, at the root of one of the aft-brackets (the one near the symmetry plane), where the pressure fluctuations have a strong component at all frequencies. This fluctuation is

5 CONCLUSION

A detailed simulation of the complex flow past a rotating propeller behind a hull in steady straight course was presented. A dynamic overlapping grid approach was exploited in order to follow the rotation of the propeller with respect to the fixed hull. The simulation was performed on two grid levels (the coarse one being obtained from the finer level by removing every other vertex along the three coordinate directions) and the numerical results were validated through high quality LDV measurements of the velocity field in the longitudinal mid–plane of the rudder and in the transversal planes behind the propeller and the rudder. The uncertainty analysis was performed both on numerical results and experimental measurements, and the deviation in the velocity and vorticity fields along a significant extraction line lies within the evaluated uncertainties. Also, the velocity and vorticity fields from EFD and CFD show an excellent agreement in both the longitudinal and transversal cuts of the field.

These comparisons yield a high confidence in the quality of the CFD simulation, and permit to examine some details that could not be resolved by EFD.

For example, the numerical data allowed to analyze the load conditions of the blades along their circular motion, highlighting the regions of maximum and minimum thrust, and to detect a zone characterized by relative high ampli-
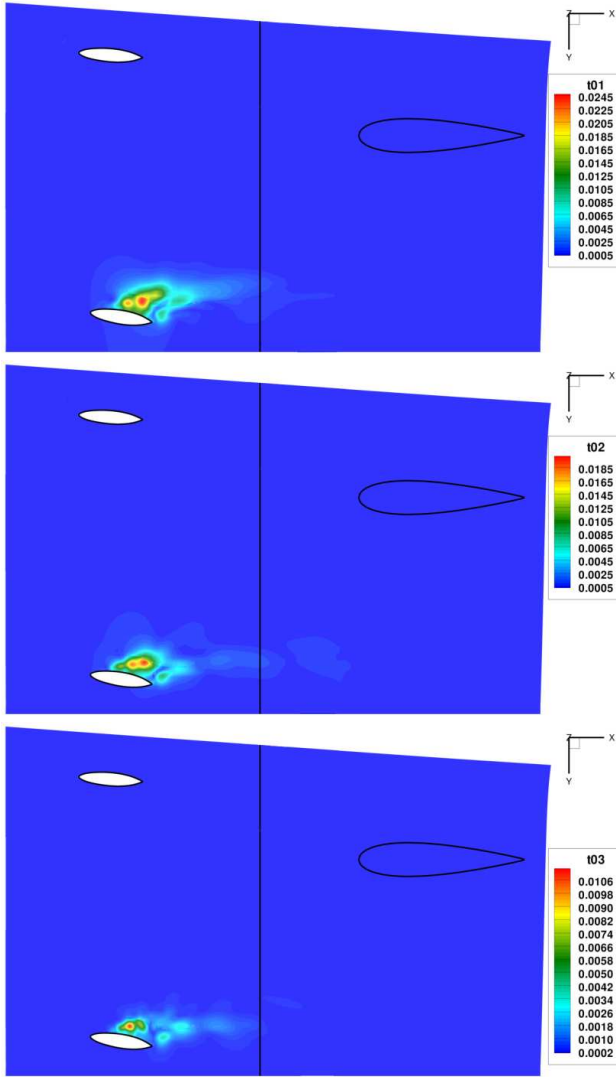
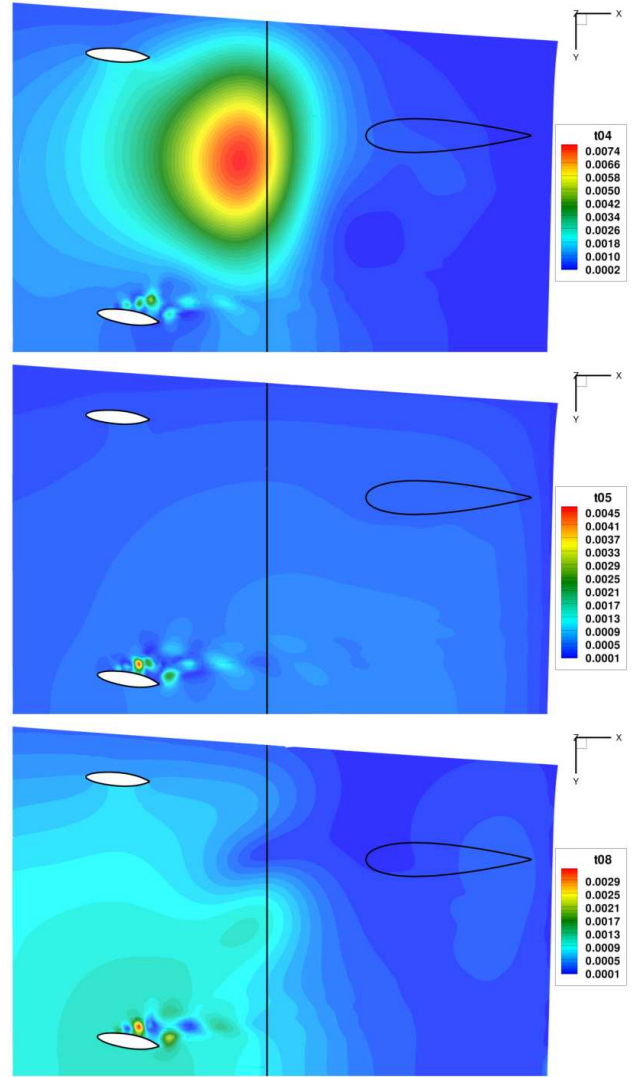Figure 18: Fourier coefficients of the pressure signal

Figure 19: Fourier coefficients of the pressure signal

tude, high frequency oscillations. These oscillations seem to depend on a detachment-reattachment phenomenon of the flow along the trailing edge of the blade, as suggested by both the pressure distribution on the surface of the propeller and the visualization of the vorticity field in the near wake of the blades.

The interaction of the wake of the propeller with the rudder, and, in particular, the behavior of the tip vortices impinging on its surface, were considered and the main features of the interaction confirm the experimental results for simpler geometries found in the literature (Felli et al 2010).

The last detailed information extracted from the simulation of the three-dimensional field concerned the pressure oscillations on the vault of the stern. This kind of data are of great relevance, for example, when problem of noise scattering is of interest. The Fourier analysis of the pressure signal on the solid surface reveals strong oscillations at all frequencies near the root of one of the shaft–brackets; these oscillations are caused by the misalignment of the bracket with the local flow direction and the consequent separation of the flow. Apart from this phenomenon, clearly indepen-

dent of the propeller motion, a large amplitude pressure oscillation at the blade frequency (and, to a minor extend, at its multiplies) is detected just ahead of the propeller plane, whereas, at other frequencies, the amplitude of the pressure signal is insignificant.

Finally, in regard to the CPU times, the simulation on the fine grid was performed on a cluster of Quad-Core AMD Opteron Processors 2352 (2.1 GHz), and was divided in 8 MPI processes each forking into 8 OpenMP threads (for a total of 64 processors). For a single revolution about 160 hours of âĂIJwall-clockâĂİ time were necessary (that is, 160*64 = 10240 CPU hours) and the whole computation took about 2,100 hours (i.e. about three months).

(Rome); their support is gratefully acknowledged.

REFERENCES

Baldwin, B. & Lomax, H. (1978). 'Thin-layer approximation and algebraic model for separated turbulent flows'. AIAA Paper 1978-257, 16th Aerospace Sciences Meeting, Huntsville, Alabama, USA.

Chang, K. C., Hsieh, W. D. & Chen, C. S. (1995). 'A Modified Low–Reynolds–Number Turbulence Model Applicable to Recirculating Flow in Pipe Expansion'. ASME J. Fluids Eng. **117**, pp. 417–423.

Di Mascio, A., Broglia, R. & Muscari, R. (2007). 'On the application of the single–phase level set method to naval hydrodynamic flows'. Comp. and Fluids **36**, pp. 868–886.

Di Mascio, A., Broglia, R. & Muscari, R. (2008). 'Numerical simulations of viscous flow around a naval combatant in regular head waves'. Proc. 6th Osaka Colloquium on Seakeping and Stability of Ships, Osaka, Japan.

Di Mascio, A., Broglia, R., Muscari, R. & Dattola, R. (2004). 'Unsteady RANS Simulation of a Manoeuvring Ship Hull'. Proceedings of the 25th Symposium on Naval Hydrodynamics, St. John's, Newfoundland and Labrador, Canada.

Felli, M., Falchi, M., Pereira, F. & Di Felice, F. (2010). 'Dynamics of the propeller wake structures interacting with a rudder'. Proceedings of the 28th Symposium on Naval Hydrodynamics, Pasadena, California, USA.

Jeong, J. & Hussain, F. (1995). 'On the identification of a vortex'. J. Fluid Mech. **285**, pp. 69–94.

Lam, C. K. G. & Bremhorst, K. (1981). 'A Modified Form of the k-epsilon Model for Predicting Wall Turbulence'. ASME J. Fluids Eng. **103**(3), pp. 456–460.

Muscari, R., Broglia, R. & Di Mascio, A. (2006). 'An overlapping grids approach for moving bodies problems'. Proceedings of the 16th International Offshore and Polar Engineering Conference (ISOPE 2006), San Francisco, California, USA.

Muscari, R. & Di Mascio, A. (2005). 'Simulation of the flow around complex hull geometries by an overlapping grid approach'. Proc. 5th Osaka Colloquium on advanced research on ship viscous flow and hull form design by EFD and CFD approaches, Osaka, Japan.

Muscari, R. & Di Mascio, A. (2009). 'Simulation of the viscous flow around a propeller using a dynamic overlapping grid approach'. Proceedings of the First International Symposium on Marine Propulsors (SMP'09), Trondheim, Norway.

Muscari, R., Felli, M. & Di Mascio, A. (2010). 'Numerical and experimental analysis of the flow around a propeller behind a fully appended hull'. Proceedings of the 28th Symposium on Naval Hydrodynamics, Pasadena, California.

Roache, P. J. (1997). 'Quantification of uncertainty in computational fluid dynamics'. Annu. Rev. Fluid Mech. **29**, pp. 123–160.

Smagorinsky, J. (1963). 'General circulation experiments with the primitive equations. I. The basic experiment'. Monthly Weather Review **91**(3), pp. 99–164.

Spalart, P. R. & Allmaras, S. R. (1994). 'A one–equation turbulence model for aerodynamic flows'. La Recherche Aérospatiale **1**, pp. 5–21.